2017 IEEE 37th International Conference on Distributed Computing Systems

PhaseBeat: Exploiting CSI Phase Data for Vital Sign Monitoring with Commodity WiFi Devices

Xuyu Wang, Chao Yang, and Shiwen Mao
Department of Electrical and Computer Engineering, Auburn University, Auburn, AL 36849-5201
Email: {xzw0029, czy0017}@auburn.edu, smao@ieee.org

***Abstract*—Vital signs, such as respiration and heartbeat, are useful to health monitoring since such signals provide important clues of medical conditions. Effective solutions are needed to provide contact-free, easy deployment, low-cost, and long-term vital sign monitoring. In this paper, we present PhaseBeat to exploit channel state information (CSI) phase difference data to monitor breathing and heartbeat with commodity WiFi devices. We provide a rigorous analysis of the CSI phase difference data with respect to its stability and periodicity. Based on the analysis, we design and implement the PhaseBeat system with off-the-shelf WiFi devices, and conduct an extensive experimental study to validate its performance. Our experimental results demonstrate the superior performance of PhaseBeat over existing approaches in various indoor environments.**

***Keywords*-Channel State Information; commodity 5GHz WiFi; health sensing; vital sign monitoring.**

I. Introduction

It is estimated that over 100 million Americans have chronic health conditions, such as lung disorders and heart diseases. Three-fourths of the total US healthcare cost are spent to treat these conditions [1], leading to an increasing demand for long-term health monitoring in indoor environments. Vital signs, such as respiration and heartbeat, are useful to physical health monitoring since such signals provide important clues of medical problems, such as sleep disorders or anomalies, and sudden infant death syndrome (SIDS) of sleeping infants [2]. Most traditional methods for vital sign monitoring require a person to wear special devices such as a capnometer [3] or a pulse oximeter [4]. These technologies are inconvenient to use and uncomfortable. Alternative solutions of contact-free, easy deployment, low-cost, and long-term vital sign monitoring would be highly appealing.

Recently, radio frequency (RF) based vital sign monitoring systems have attracted great interest, which exploits wireless signals to detect breathing-induced chest movement. For example, the Vital-Radio system uses a frequency modulated continuous wave (FMCW) radar to estimate breathing and heart rates [5]. It works for multiple subjects in parallel, but requires a customized hardware with a large bandwidth from 5.46 GHz to 7.25 GHz. Other techniques, such as the Doppler radar [6], [7] and the ultra-wideband radar [8], are also incorporated to monitor vital signs, which also require dedicated hardware with large bandwidth and high cost. The mmVital system [9] uses the received signal strength (RSS) of 60 GHz millimeter wave (mmWave) signals for breathing and heart rates estimation with a larger bandwidth about 7GHz, which also requires customized hardware and a mechanical rotator. A recent work UbiBreathe monitors the breathing signal using WiFi RSS, which is coarse channel information [10]. UbiBreathe requires a line of sight (LOS) path between the transmitter and receiver, which limits the RF monitoring range in the deployment environment.

Unlike RSS, the channel state information (CSI) represents fine-grained channel information, which is now available for several off-the-shelf WiFi network interface cards (NIC), e.g., Intel WiFi Link 5300 NIC [11] and the Atheros AR9580 chipset [12]. Specifically, CSI consists of both subcarrier-level amplitude and phase information of the orthogonal frequency division multiplexing (OFDM) channel. It is a more stable representation of channel characteristics than RSS. In a recent work [13], the authors use the amplitudes of WiFi CSI data to track vital signs of a sleeping person. However, the CSI phase information has not been used for vital sign monitoring so far, due to large variations caused by noise and the unsynchronized time and frequency at the transmitter and receiver.

In this paper, we leverage CSI phase difference data between two antennas of the receiver NIC to detect and monitor breathing rate and heart rate. We find that the CSI phase difference data is quite stable after suitable calibration. Moreover, the CSI phase difference data is also more robust than RSS in various deployment scenarios, such as different distances, obstacles/walls, and orientations. We provide a rigorous analysis of CSI phase difference data, and prove that for indoor multipath environments under small-scale fading, the CSI phase difference data is a periodic signal with the same frequency as the breathing signal, when the wireless signal is reflected from the chest of a person.

Built upon the analysis, we design PhaseBeat, a remote sensing system using CSI phase difference data for monitoring respiration and heartbeat with commodity WiFi device. First, PhaseBeat exploits the CSI phase difference data to extract the periodic signal induced by chest movements (e.g., inhaling and exhaling). Then, PhaseBeat preprocesses the captured data, with environment detection, data calibration,

1063-6927/17 $31.00 © 2017 IEEE
DOI 10.1109/ICDCS.2017.206

subcarrier selection, and discrete wavelet transform. The cleansed CSI phase difference data is then used to estimate the breathing and heart rate in realtime. We implement PhaseBeat with off-the-shelf WiFi devices and evaluate its performance with extensive experiments, which involve four persons over three months in typical indoor environments, such as a computer laboratory, a through-wall scenario, and a long corridor. The experimental results demonstrate that PhaseBeat can achieve high accuracy for breathing and heart rate estimation, with median error of 0.25 bpm and 1 bpm, respectively. We also find PhaseBeat highly robust for breathing rate estimation under various environments, such as different distances between the transmitter and receiver.

In the remainder of this paper, we present the preliminaries and our analysis of phase difference data in Section II. We describe the PhaseBeat design in Section III and demonstrate its performance in Section IV. Section V reviews related work and Section VI concludes this paper.

II. Preliminaries and Phase Difference Analysis

A. Channel State Information Preliminaries

OFDM is widely used in modern wireless network standards, such as WiFi (i.e., IEEE 802.11a/g/n). With OFDM, the total spectrum is partitioned into multiple orthogonal subcarriers, and wireless data is transmitted over the subcarriers using the same modulation and coding scheme (MCS) to mitigate frequency selective fading. Leveraging the device driver for off-the-shelf NICs, e.g., the Intel 5300 NIC [11], we can extract the CSI from the NIC, which is fine-grained physical layer (PHY) information. CSI reveals the channel characteristics experienced by the received signal such as the multipath effect, shadow fading, and distortion [26], [27].

With OFDM, the WiFi channel at the 5 GHz band can be considered as a narrowband flat fading channel. In the frequency domain, the channel model can be expressed as $\vec{Y} = \text{CSI} \cdot \vec{X} + \vec{N}$, where $\vec{Y}$ and $\vec{X}$ denote the received and transmitted signal vectors, respectively, $\vec{N}$ is the additive white Gaussian noise, and CSI represents the channel's frequency response, which can be estimated from $\vec{Y}$ and $\vec{X}$.

Although the WiFi OFDM system has 56 subcarriers over a 20 MHz channel, the Intel 5300 NIC can report CSI for only 30 of the 56 subcarriers. The channel frequency response of subcarrier i, CSI_i, is a complex value, that is

$$\text{CSI}_i = \mathcal{I}_i + j\mathcal{Q}_i = |\text{CSI}_i| \exp(j\angle \text{CSI}_i), \tag{1}$$

where $\mathcal{I}_i$ and $\mathcal{Q}_i$ are the in-phase component and quadrature component, respectively; $|\text{CSI}_i|$ and $\angle\text{CSI}_i$ are the amplitude response and phase response of subcarrier i, respectively.

For an indoor environment with NLOS components [14], the channel frequency response of subcarrier i can also be formulated as

$$\text{CSI}_i = \sum_{k=0}^{K} r_k \cdot e^{-j2\pi f_i \tau_k}. \tag{2}$$

where K is the number of multipaths, r_k and τ_k are the attenuation and the propagation delay from the k_{th} path, respectively, and f_i is the central frequency of subcarrier i. Traditionally, the multipaths are harmful for indoor localization, because only the LOS component is a good indicator of distance [14], [15]. However, our PhaseBeat system can effectively exploit the reflections for vital signals monitoring, as will be shown in this paper.

B. Phase Difference Information

In this section, we show that the CSI phase difference data between two antennas for consecutive packets of the 5 GHz OFDM channel is highly stable and a periodic signal with the same frequency as the breathing signal. We now provide an analysis to validate the stability from the measured phase difference. Let $\angle\widehat{CSI}_i$ denote the measured phase of subcarrier i, which is given by [12], [16], [23]–[25]

$$\angle\widehat{CSI}_i = \angle\text{CSI}_i + (\lambda_p + \lambda_s)m_i + \lambda_c + \beta + Z, \tag{3}$$

where $\angle\text{CSI}_i$ is the true phase value, m_i is the subcarrier index of subcarrier i, β is the initial phase offset due to the phase-locked loop (PLL), Z is the measurement noise that is assumed to be AWGN of variance σ^2, and λ_p, λ_s and λ_c are the phase errors from the packet boundary detection (PBD), the sampling frequency offset (SFO), and central frequency offset (CFO), respectively [16]. The phase errors can be written as

$$\lambda_p = 2\pi\frac{\Delta t}{N}, \lambda_s = 2\pi\left(\frac{T'-T}{T}\right)\frac{T_s}{T_u}n, \lambda_c = 2\pi\Delta f T_s n, \tag{4}$$

where Δt is the packet boundary detection delay, N is the FFT size, T' and T are the sampling periods at the receiver and the transmitter, respectively, T_u is the length of the data symbol, T_s is the total length of a data symbol and the guard interval, n is the sampling time offset for the current packet, and Δf is the center frequency difference between the transmitter and receiver. Note that we cannot obtain the exact values for Δt, $\frac{T'-T}{T}$, n, Δf, and β in (3) and (4). Moreover, λ_p, λ_s, and λ_c vary for different packets with different Δt and n. Thus, the true phase $\angle\text{CSI}_i$ cannot be derived from the measured phase value. Fortunately, the measured *phase difference* on subcarrier i can be leveraged as in the following theorem.

Theorem 1. *The measured phase difference on subcarrier i between two receiver antennas is stable, and its mean and variation are given by*

$$\begin{cases} \mathbb{E}(\Delta\angle\widehat{CSI}_i) = \mathbb{E}(\Delta\angle CSI_i) + \Delta\beta \\ \text{Var}(\Delta\angle\widehat{CSI}_i) = \text{Var}(\Delta\angle CSI_i) + 2\sigma^2. \end{cases} \tag{5}$$

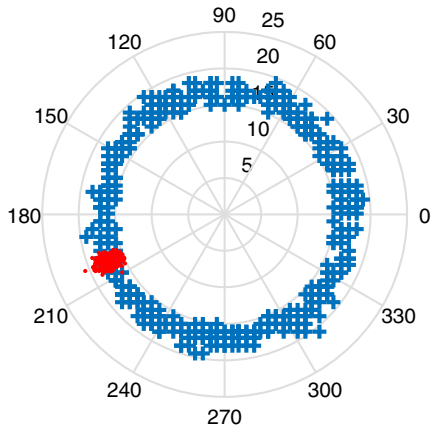

Figure 1. Comparison between phase CSI measured from a single antenna (marked as blue crosses) and the phase differences measured from two antennas (marked as red dots) of the 5th subcarrier for 600 consecutively received packets.

Proof: Note that the three antennas of the Intel 5300 NIC use the same clock and the same down-converter frequency. Consequently, the measured phases of subcarrier i from two antennas have identical packet detection delay, sampling periods, frequency differences, and the same index m_i [17]. Thus the measured phase difference on subcarrier i between two antennas can be approximated as

$$\Delta\angle\widehat{CSI}_i = \Delta\angle\text{CSI}_i + \Delta\beta + \Delta Z, \tag{6}$$

where $\Delta\angle\text{CSI}_i$ is the true phase difference of subcarrier i, $\Delta\beta$ is the unknown difference in phase offsets, which is in fact a constant [17], and ΔZ is the noise difference with variance $2\sigma^2$. Since Δt, Δf, and n are all removed, $\Delta\angle\widehat{CSI}_i$ in (6) becomes highly stable for consecutive packets. From (6), we can derive the mean and variance of the measured phase difference on subcarrier i as that given in (5). ■

From (6), it can be seen that $\mathbb{E}(\Delta\angle\widehat{CSI}_i) - \mathbb{E}(\Delta\angle\text{CSI}_i)$ is a constant $\Delta\beta$. The difference does not change the estimated frequency of vital signals, although its variance becomes larger. Fig. 1 is a comparison between the single antenna phases (as blue crosses) and the phase differences (as red dots) of the 5th subcarrier in the polar coordinate plot for 600 consecutively received packets. We can see that the single antenna phase of the 5th subcarrier is nearly uniformly distributed between $0°$ and $360°$, making it unusable. However, all phase difference data of the 5th subcarrier concentrate into a sector between $190°$ and $210°$, which clearly validates Theorem 1.

In the following Theorem, we show the measured phase difference information is periodic.

Lemma 1. *When the wireless signal is reflected from the chest of a person with a breathing frequency f_b, the true phase of the reflected signal at any antenna of the receiver is also periodic with the same frequency f_b.*

Proof: Because the wireless signal on subcarrier i is a plane wave, its true phase at the receiver is determined by the propagation distance, that is $\angle\text{CSI}_i = 2\pi d(t)/\lambda_i$, where $d(t)$ is the propagation distance at time t and λ_i is the wavelength of subcarrier i. When the chest of a person periodically rises and falls with frequency f_b, the propagation distance $d(t)$ of the reflection signal becomes $d(t) = D + A\cos(2\pi f_b t)$, where D is the constant mean distance of the reflection path, A is the amplitude of the periodic signal from chest movements. Thus, the true phase of the reflected signal at the receiver is $\angle\text{CSI}_i = 2\pi(D + A\cos(2\pi f_b t))/\lambda_i$. Clearly, the true phase at the receiver is a periodic signal with the frequency f_b. ■

Theorem 2. *For indoor environments with multipaths, when the wireless signal is reflected from the chest of a person with breathing frequency f_b, the true phase at any antenna of the receiver is also a periodic signal with frequency f_d such that*

$$P\left(|f_d - f_b| < \epsilon\right) = 1, \quad \forall \epsilon > 0. \tag{7}$$

The proof is omitted for brevity.

In the following section, we describe the design of the PhaseBeat system, aiming to overcome the above challenges for estimating breathing rate and heart rate using CSI phase difference data, for one or more persons.

III. The PhaseBeat System

A. PhaseBeat System Architecture

We design the PhaseBeat system to monitor vital signs such as breathing and heartbeat of one or more persons by leveraging CSI phase difference data with commodity WiFi devices. Specifically, PhaseBeat exploits CSI phase difference data to extract the periodic signal caused by the rise and fall of the chest (e.g., inhaling and exhaling). Based on Theorems 1 and 2, PhaseBeat can effectively exploit CSI phase difference data to monitor vital signs. First, CSI phase difference data is relatively stable for back-to-back packets in stationary environments such as people sitting, standing, or sleeping. It can thus be effective for monitoring vital signs. Second, CSI phase difference data includes the periodic signal that has the same frequency as the breathing signal. Finally, the CSI phase difference data is more robust, with only small variations for different distances or different orientations, compared with CSI amplitude data used in prior work for monitoring vital signs.

The PhaseBeat system architecture is presented in Fig. 2. It includes four basic modules: Data Extraction, Data Preprocessing, Breathing Rate Estimation, and Heart Rate Estimation. The Data Extraction module extracts CSI phase difference data between two receive antennas of an off-the-shelf WiFi device. The Data Preprocessing module consists of

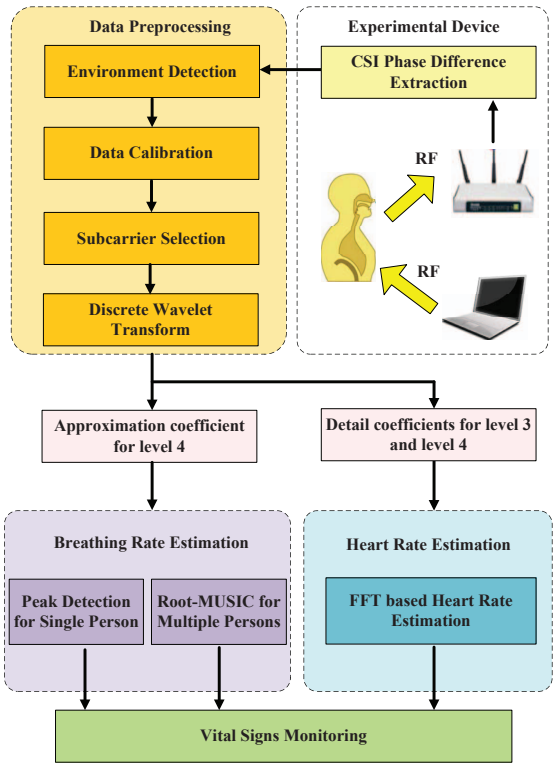

Figure 2. PhaseBeat system architecture.

environment detection, data calibration, subcarrier selection, and discrete wavelet transform. For environment detection, we adopt a threshold method to determine the stationary states of a person, such as sitting, standing, or sleeping. For data calibration, we remove the direct current (DC) component and high frequency noises, and downsample the processed data. Then, subcarrier selection is used to improve the reliability of CSI phase difference data. The discrete wavelet transform (DWT) is used to obtain the denoised breathing signal with approximation coefficient for level 4 and the reconstructed heart signal with the sum of detail coefficients for level 3 and level 4. In the Breathing Rate Estimation module, we use peak detection for the case of a single person and the root-MUSIC method for the case of multiple persons. In the Heart Rate Estimation module, we use an FFT based method to detect the heart rate.

B. Data Preprocessing

1) Environment Detection: After extracting the CSI phase difference information using (6), we need to determine whether the person is in a stationary state. When the person is determined to be in a stationary state, such as sitting, standing, or sleeping, PhaseBeat can estimate his/her breathing rate and heart rate. A threshold-based method is used to identify whether a segment of CSI phase difference data is received in a stationary state, by computing the mean absolute deviation of the CSI phase difference data in a short sliding window.

We define V as the sum of mean absolute deviations of all CSI phase difference data in the sliding window as

$$V = \frac{1}{|W|} \sum_{i=1}^{30} \sum_{k \in W} |\Delta\angle\widehat{CSI}_i(k) - \mathbb{E}(\Delta\angle\widehat{CSI}_i(k))|, \quad (8)$$

where $\Delta\angle\widehat{CSI}_i(k)$ is the measured phase difference from subcarrier i for packet k, W is the index set of all the packets in the sliding window, $|W|$ is the length of the sliding window. Because other movement events lead to larger variations in CSI phase difference data than that caused by the minute movements of breathing and heartbeat, the threshold-based approach is effective to detect such large movements (such as walking or jumping). In PhaseBeat, we set the threshold between 0.25 and 6 to identify useful data for vital sign monitoring. Fig. 3 shows the environment detection results for different states. When the person is sitting, the phase difference data is a sinusoidal-like periodic signal over time. When there is no one in the range, the phase difference data is a straight line with very small fluctuations. When the person stands up or is walking, the phase difference data exhibits larger fluctuations. Thus, a simple threshold can be effective to determine the stationary state of the person.

2) Data Calibration: To obtain robust CSI phase difference data, we further perform data calibration to remove the DC component and high frequency noises, and to downsample the processed data. First, because the DC component affects subcarrier selection, peak detection, and FFT frequency estimation, PhaseBeat needs to remove the DC component with the Hampel Filter. Unlike traditional data calibration methods that only remove high frequency noises, we use the Hampel Filter for detrending of the original CSI phase difference data to remove the DC component. The Hampel Filter is utilized to obtain the basic trend of the original data, which is set as a large sliding window with 2000 samples and a small threshold of 0.01. Then, the detrended data is obtained by subtracting the basic trend data from the original data. In addition, we also leverage the Hampel Filter to reduce high frequency noises using a smaller sliding window with 50 samples and the same threshold of 0.01. Second, because PhaseBeat employs a data sample rate of 400 Hz, we need to implement downsampling to reduce the computation complexity for realtime breathing and heart rate estimation. We use a sampling interval of 20 to obtain the low frequency CSI phase difference data, that is equivalent to sampling at 20 Hz.

Fig. 4 presents the data calibration results. It can be seen that the original phase differences of all subcarriers have a DC component and high frequency noises. By implementing the proposed data calibration scheme, both the DC component and high frequency noises are removed; the CSI from each of the subcarriers becomes a sinusoidal-like periodic

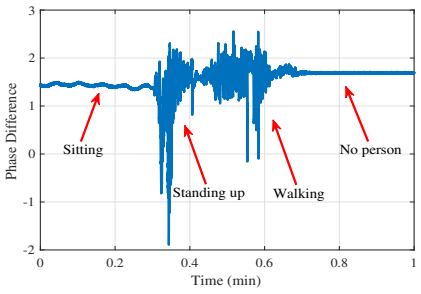

Figure 3. Environment detection.

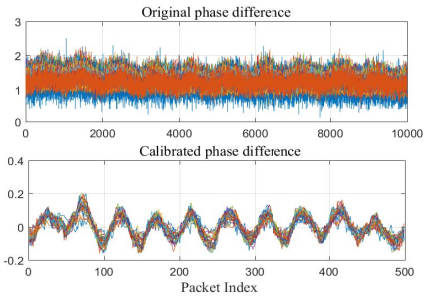

Figure 4. Data calibration.

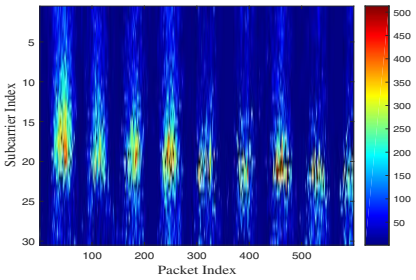

Figure 5. CSI phase difference series patterns after data calibration.

signal over the packets with low noise; and the number of packets is decreased from 10000 to 500, which is amenable to applying other signal processing methods.

3) Subcarrier Selection: PhaseBeat employs subcarrier selection to further boost the reliability of CSI phase difference data, because different subcarriers have different wavelengths, leading to the different sensitivity for breathing and heart signals. We use the mean absolute deviation of CSI phase difference data from every subcarrier to measure its sensitivity. Generally the larger the mean absolute deviation, the higher the sensitivity. Thus, we first choose k maximum mean absolute deviations of CSI phase difference data. Then, we use the median of the k mean absolute deviations of CSI phase difference data to make the final selection. Fig. 5 shows the CSI phase difference series patterns after data calibration. We can see that the neighboring subcarriers of subcarrier 20 have higher sensitivity to breathing signals. Then, as shown in Fig. 7, the mean absolute deviation of CSI phase difference data of subcarrier 19 is the maximum. In PhaseBeat, we set the $k = 3$ as the default value, and subcarriers 19, 18, and 2 are thus selected. With the above approach, subcarrier 18 is finally selected, which has the highest sensitivity as shown in Fig. 7.

4) Discrete Wavelet Transform (DWT): Different from FFT and short time Fourier transform (STFT), DWT can achieve a time-frequency representation of data, which provides not only the optimal resolution both in the time and frequency domains, but also a multi-scale analysis of the data. With DWT, the phase difference data after subcarrier selection can be decomposed into an *approximation coefficients* vector with a low-pass filter and a *detail coefficients* vector with a high-pass filter. In fact, the approximation coefficient vector represents the basic shape of the input signal with large scale characteristics, while the detail coefficient vector describes the high frequency noises and the detailed information with small scale characteristics.

In wavelet decomposition, the following steps recursively split the previous approximation coefficient and detail coefficient into two new coefficients based on the same scheme [18]. After L steps, the DWT can obtain an approximation coefficient α^L and a sequence of detail coefficients $\beta^1, \beta^2, ..., \beta^L$. We can compute the DWT coefficients as follows.

$$\begin{cases} \alpha_k^{(L)} = \sum_{n\in\mathbb{Z}} \Delta\angle\widetilde{CSI}(n)\phi_{n-2^L k}^{(L)}, \ L \in \mathbb{Z} \\ \beta_k^{(l)} = \sum_{n\in\mathbb{Z}} \Delta\angle\widetilde{CSI}(n)\psi_{n-2^l k}^{l}, \ l \in \{1, ..., L\}, \end{cases} \tag{9}$$

where $\Delta\angle\widetilde{CSI}(n)$ is the phase difference data after subcarrier selection, $\mathbb{Z}$ is the integer set, the ϕ's and ψ's are wavelet basis functions, which are orthogonal to each other. The phase difference data $\Delta\angle\widetilde{CSI}(n)$ can be approximated using inverse DWT, as

$$\Delta\angle\widetilde{CSI}(n) = \sum_{k\in\mathbb{Z}} \alpha_k^{(L)}\phi_{n-2^L k}^{(L)} + \sum_{l=1}^{L}\sum_{k\in\mathbb{Z}} \beta_k^{(l)}\psi_{n-2^l k}^{l}. \tag{10}$$

In PhaseBeat, DWT is employed to remove high frequency noises from the collected CSI phase difference data. Moreover, the approximation coefficient α^L is used to detect the breathing rate, while the sum of detail coefficients $\beta^{L-1} + \beta^L$ is used to detect the heart rate. We set L to 4 in this paper. As shown in Fig. 6, for the original signal, we first implement the DWT based decomposition recursively for four levels with the Daubechies(db) wavelet filter. Because we obtain a 20 Hz sampling rate after data calibration, and the sampling rate is halved after every step of decomposition, the detail coefficient β^1 and the approximation coefficient α^1 have a frequency ranging from 10 Hz to 5 Hz and 0 Hz to 5 Hz, respectively. Then, the approximation coefficient α^4 has a frequency in 0 Hz to 0.625 Hz to obtain the denoised breathing signal. The sum of detail coefficients $\beta^3 + \beta^4$ has the range from 0.625 Hz to 2.5 Hz to reconstruct the heart signal.

C. Breathing Rate Estimation

1) Peak Detection for the One Person Case: The breathing signal is caused by the small, periodic movement of inhaling and exhaling, which can be extracted from the phase difference data according to Theorem 2. Although the FFT based method can be used to estimate the breathing rate, the accuracy may not be good. This is because the frequency resolution depends on the window size of FFT. If the window size becomes larger, the estimation accuracy

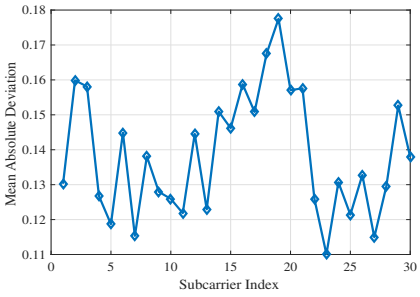

Figure 7. Mean absolute deviation of each subcarrier.

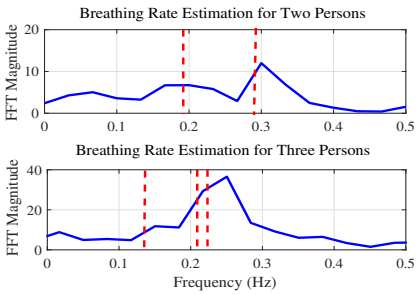

Figure 8. Breathing rate estimation for two persons (the upper plot) and three persons (the lower plot) based on FFT.

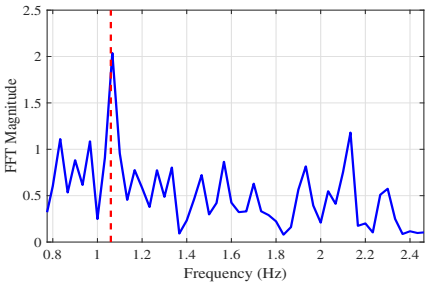

Figure 9. Heart rate estimation based on FFT.

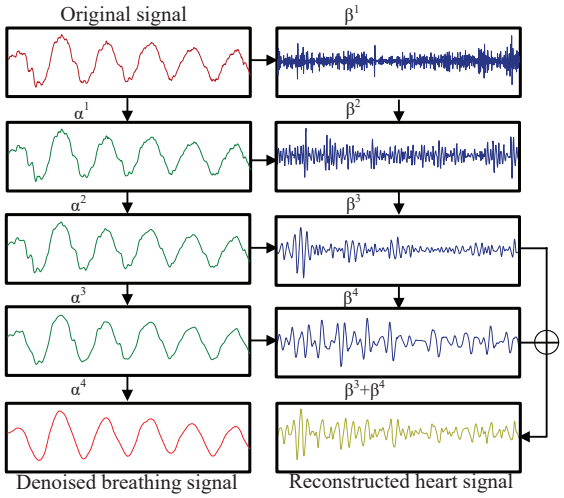

Figure 6. Discrete wavelet transform results.

will be higher, but the larger window size also leads to a lower time domain resolution. Therefore, our PhaseBeat system employs peak detection to estimate the breathing rate based on the approximation coefficient α^L to achieve high accuracy.

However, we find that the approximation coefficient α^L still has fake peaks (i.e., local maximums). We thus use the sliding window method to identify the true peak, where the window size is set to 51 samples based on human's maximum breathing period [13]. Then, we can identify all the peaks by checking whether the median of all the samples in the window is the maximum value or not. After peak detection, all peak-to-peak intervals are averaged to obtain the period of the breathing signal, denoted as P. Finally, the estimated breathing rate can be computed as $60/P$ bpm.

2) Root-MUSIC for Multiple Person Case: An FFT based method can transform the approximation coefficient α^L from the time domain to the frequency domain to estimate the breathing frequencies for two persons in LOS environments. However, with more persons and more cluttered environments, the FFT based method always leads to poor results, especially when there are two or more breathing rates very close to each other. Fig. 8 illustrates the breathing rate estimation for two persons (the upper plot) and three persons (the lower plot) with the FFT method, where the red dotted lines mark the real breathing frequencies (i.e., the ground truth). We can see that the estimated frequencies for the two persons are 0.2 Hz and 0.3 Hz, respectively, which are both quite accurate. However, for the case of three persons, the FFT curve only shows two peaks, and the estimated breathing rates are much less accurate.

To address this issue, we propose a root-MUSIC method to estimate multiple breathing rates based on phase difference data. In fact, we leverage 30 CSI phase difference series patterns after data calibration to build the estimated correlation matrix $\widehat{\mathbf{R}}$, which is given by

$$\widehat{\mathbf{R}} = \mathbf{H}\mathbf{H}^T, \tag{11}$$

where $\mathbf{H}$ is a matrix that represents 30 CSI phase difference series after data calibration, which is defined as

$$\mathbf{H} = \begin{bmatrix} h_1(1) & h_2(1) & \cdots & h_{30}(1) \\ h_1(2) & h_2(2) & \cdots & h_{30}(2) \\ \vdots & \vdots & \cdots & \vdots \\ h_1(I) & h_2(I) & \cdots & h_{30}(I) \end{bmatrix}, \tag{12}$$

where $h_i(j)$ is the phase difference from subcarrier i for packet j after data calibration, and I is the total number of packets. After obtaining the estimated correlation matrix $\mathbf{R}$, we incorporate the standard root-MUSIC method to obtain multiple persons breathing frequencies, which is effective for estimating frequencies of signals consisting of a sum of sinusoids with additive white Gaussian noise [19]. For the same phase difference data for three persons in Fig. 8, the breathing frequencies estimated by the proposed method are 0.1467 Hz, 0.2233 Hz, and 0.2483 Hz, respectively, which are much more accurate than those estimated by the FFT based on method. Moreover, we can see that the proposed root-MUSIC method can effectively distinguish two close breathing frequencies.

D. Heart Rate Estimation

1) FFT Based Heart Rate Estimation: Heart rate is an important indicator of health condition and vital sign. Similar

to the breathing signal, the heart signal is also periodic, but its magnitude is extremely weak. Usually, breathing signal is orders of magnitude stronger than the heart signal. The movement of the heart (i.e., diastole and systole) only causes small variations in the reflected signal. Moreover, the much stronger breathing signal also generates higher harmonics, which becomes strong interferences to the heart signal. It is thus more challenging to detect the heart rate than the breathing rate.

In PhaseBeat, we employ a directional antenna at the transmitter to improve the power of the reflected signal. Then, the sum of the detail coefficients $\beta^{L-1} + \beta^{L}$ of the wavelet decomposition is utilized to estimate the heart rate. When the level of decomposition is $L = 4$, the frequency range is between 0.625 Hz and 2.5 Hz, which filters out the breathing signals, which are between 0.17 Hz and 0.62 Hz, as well as higher frequency noises. Finally, we can use an FFT based method to transform the sum of the detail coefficients $\beta^{L-1} + \beta^{L}$ to the frequency domain to estimate the heart rate. To improve the frequency resolution, we adopt the method proposed in [5] for heart rate estimation. After finding the peak of FFT, we use the three bins, including the peak bin and its two adjacent bins, where an inverse FFT is performed to obtain a complex time-domain signal. The heart rate is estimated by evaluating the phase of the signal. Fig. 9 shows the heart rate estimation with FFT. The PhaseBeat estimated heartbeat frequency is 1.07 Hz, while heartbeat frequency measured by a commercial fingertip pulse sensor is 1.06 Hz. The heart rate estimated error is 0.01 Hz, or 0.6 bpm, in this experiment.

IV. Experimental Study

A. Test Configuration

In this section, we present our extensive experimental study with PhaseBeat in the 5 GHz band. In the experiments, we use a desktop computer as an access point and a Lenovo laptop as a mobile device, both equipped with the Intel 5300 NIC. Our PhaseBeat system is implemented on the Ubuntu desktop 14.04 LTS OS for both the access point and the mobile device. The access point operates in the *monitor mode* and the distance between two adjacent antennas is $d = 2.68$ cm, which is half of the wavelength in the 5 GHz band. The mobile device operates in the *injection mode*, to transmit packets at 400 packets per second using only one antenna. Then, we extract CSI phase difference data between two adjacent antennas at the access point for vital signal estimation.

We conducted extensive experiments with PhaseBeat with four persons over three months. The test scenarios include a computer laboratory and corridors as shown in Fig. 10. We have three setups in these two environments for the results reported in this paper. The first setup is within the *laboratory*, a 4.5×8.8 m^2 room. The room is crowed with tables and PCs, which block part of the LOS paths and

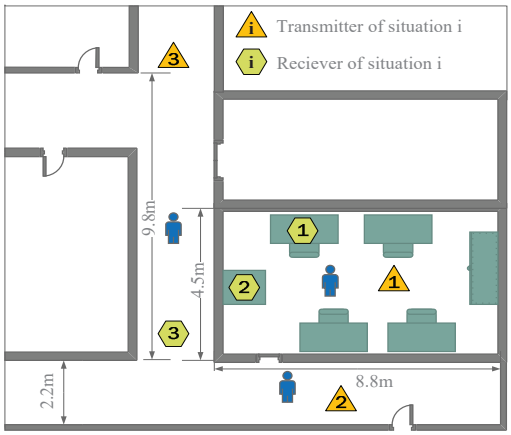

Figure 10. Experimental setup scenarios.

form a complex radio propagation environment. The second setup is a *through-wall* scenario, where the person is on the transmitter side, separated by a wall from the receiver. The third setup is the 20 m *long corridor*, where the receiver and the transmitter are 11 m apart. We use omnidirectional antennas at both the receiver and transmitter for breathing rate estimation in all the three scenarios. We use a directional antenna at the transmitter in the laboratory scenario for heart rate estimation. For comparison purpose, we employ the NEULOG Respiration Monitor Belt Logger Sensor and a fingertip pulse oximeter to record the ground truths of the breathing and heart rates.

B. Performance of Breathing and Heart Rate Estimation

Fig. 11 presents the cumulative distribution functions (CDF) of estimation error in breathing rate estimation. We use the amplitude based method [13] as a benchmark in this experiment. We can see that both systems have a similar median estimate error at about 0.25 bpm. However, we can see that for PhaseBeat, 90% of the test data have an estimated error under 0.5 bpm, while 70% of the test data for the amplitude based method have an estimated error under 0.5 bpm. Moreover, the maximum estimation error for PhaseBeat and the amplitude based method are 0.85 bpm and 1.7 bpm, respectively. Therefore, our PhaseBeat system achieves a considerably higher accuracy than the amplitude based method for breathing rate estimation.

Fig. 12 presents the CDF of estimation error in heart rate estimation. For heart signal detection, we need to use the directional antenna at the transmitter to improve the received power. We can see that the variation of CSI phase difference data becomes larger, while the variation of CSI amplitude data becomes small, although we cannot directly see the periodic heart signal. Thus, we only show the PhaseBeat results for heart signal estimation. In Fig. 12, we find that PhaseBeat has a median estimate error of about 1 bpm, while 80% of the test data have an estimated error under 2.5 bpm. Moreover, the maximum estimation error for PhaseBeat is

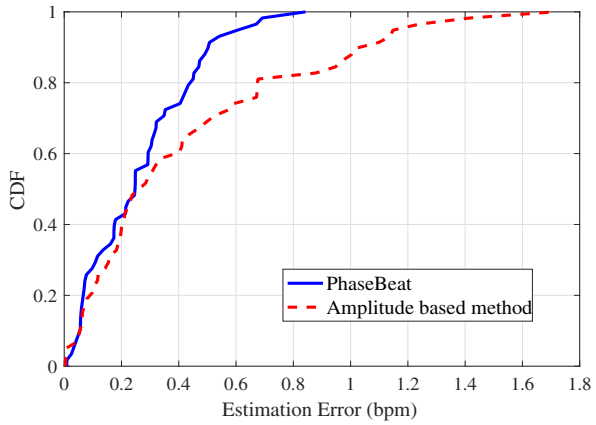

Figure 11. CDFs of estimation error in breathing rate estimation.

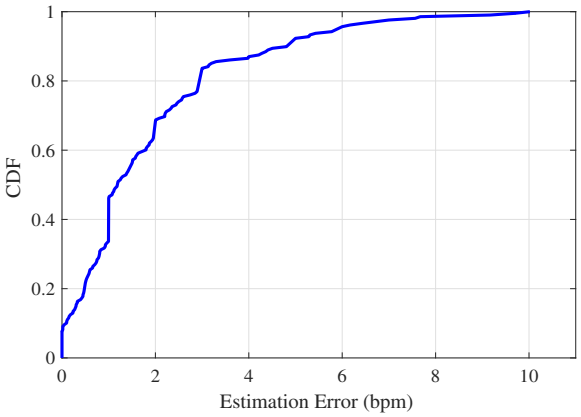

Figure 12. CDFs of estimation error in heart rate estimation.

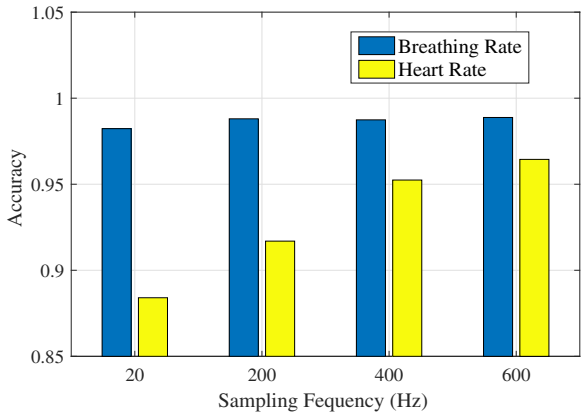

Figure 13. Accuracy of breathing and heart rates estimation for different sampling frequency.

about 10 bpm. We notice that the estimated accuracy of heart rate is lower than the breathing rate estimation because of the much weaker heart signal.

Fig. 13 shows the accuracy of breathing and heart rates estimation for different sampling frequencies. For data calibration, we adopt a 400 Hz sampling frequency to estimate

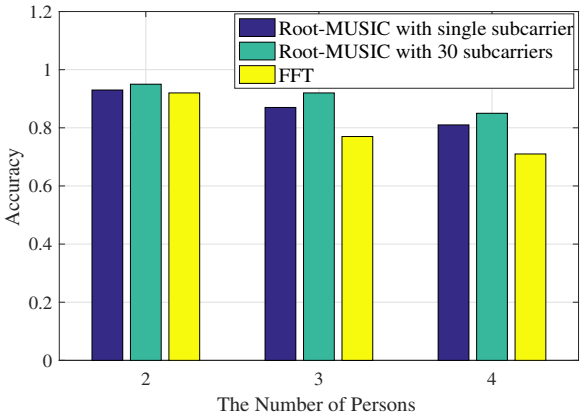

Figure 14. Accuracy of breathing rates estimation for different number of persons.

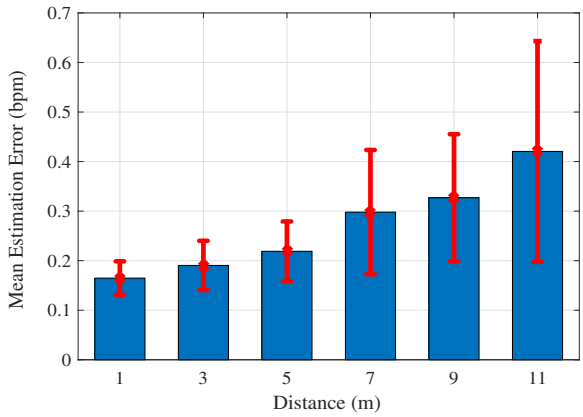

Figure 15. Impact of the distance between the transmitter and the receiver for the long corridor.

the vital signs, which is sufficient to accurately detect the heart signal. As shown in Fig. 13, the breathing rate estimation have a similar high accuracy of about 98% for different sampling frequencies. However, the accuracy of the heart rate estimation is only 88% for a sampling frequency of 20 Hz, while it can achieve an accuracy of 95% with the 400 Hz sampling rate. Thus, we choose the 400 Hz sampling rate for PhaseBeat, which is used for all the experimental results in this paper.

Fig. 14 shows the accuracy of breathing rates estimation for different numbers of persons. Moreover, we compare the proposed root-MUSIC method using 30 subcarriers with the FFT based method, and with root-MUSIC method using a single subcarrier. It is noticed that for multiple persons, the accuracy of breathing rate estimation decreases for all the three schemes. Moreover, we can see that for two-person breathing rates estimation, the three methods all have a high accuracy above 90%. However, for four persons breathing rate estimation, the root-MUSIC method using 30 subarriers have the best performance among the three.

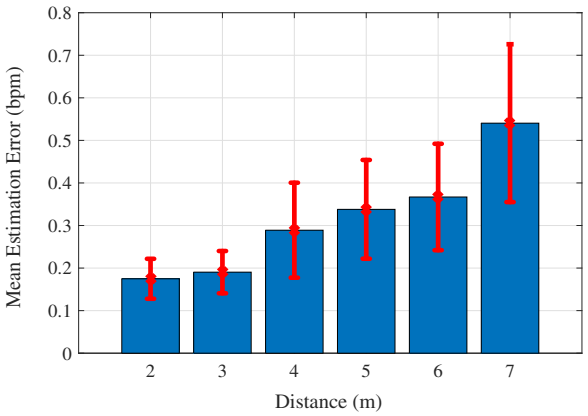

Figure 16. Impact of the distance between the transmitter and the receiver for through-wall scenario.

C. Impact of the Transmitter-Receiver Distance

Fig. 15 and Fig. 16 show the impact of the distance between the transmitter and the receiver for the long corridor and through-wall scenario, respectively. When the distance between the transmitter and the receiver is increased, the mean estimation error is also increased. This is because the reflected signal is reduced when the distance between the transmitter and receiver is long, which influences the dynamic range of phase difference data. Moreover, we can see that the mean estimation error at the same distance for the through-wall scenario is larger than that for the long corridor scenario. For example, when the distance is 7 m, the mean estimation errors for the long corridor and the through-wall scenario are 0.3 bpm and 0.52 bpm, respectively. It is because the signal for the through-wall scenario has a larger attenuation than that for the long corridor scenario.

V. Related Work

This work is closely related to two categories of vital sign monitoring, i.e., sensor based and RF signal based systems, which are discussed in the following.

Sensor based systems for vital sign monitoring leverage special hardware attached to the human body. Typically, special devices, such as a capnometer that can measure carbon dioxide (CO2) concentrations in respired gases, are used to monitor patients' breathing rate in hospitals [3]. However, it is very uncomfortable to wear, and is mainly used in clinical environments. Photoplethysmography (PPG) is an optical technique to measure the blood volume variations in the tissues by detecting the changes in light absorption, which requires the sensors to be attached to the patient's finger (e.g., pulse oximeters) [4]. Moreover, smartphone can utilize the embedded camera to measure light changes from the video frames. Then, the pixel of the frame is transformed into RGB components, which can detect the PPG signal to estimate the heart rate [20]. Recently, the smartphones can measure the breathing rate with the built-in accelerometer, gyroscope [21], and microphone [22], which require the user to place the smartphone near the body and wear sensors. These techniques all require attached sensors, which cannot be applied for remote monitoring of vital signs.

RF based systems for vital sign monitoring exploit wireless signals to extract the breathing-induced chest movements, which is mainly based on radar and WiFi techniques. For radar based vital sign monitoring, some techniques such as the Doppler radar [6], [7] and the ultra-wideband radar [8] are developed, which require special hardware with high frequency and high cost. A recent work employs a frequency modulated continuous wave (FMCW) radar to estimate breathing and heart rates, even for multiple subjects in parallel [5]. However, this system requires customized hardware with a large bandwidth from 5.46 GHz to 7.25 GHz. For WiFi based vital signs monitoring, UbiBreathe uses WiFi RSS for breathing rate estimation, which requires the device be placed along the LOS path between the transmitter and the receiver for monitoring the breathing signal [10]. Furthermore, based on RSS, mmVital uses 60 GHz millimeter wave (mmWave) signals for breathing and heart rates estimation using a larger bandwidth about 7 GHz [9]. This techniques does not work over a relatively longer distance and requires a high gain directional antenna at both the transmitter and the receiver. Recently, the authors in [13] exploit the amplitudes of CSI data of WiFi to track vital signs. This work is focused on monitoring breathing and heart rates when one person is sleeping.

The PhaseBeat system is motivated by these interesting prior works. To the best of our knowledge, it is the first to leverage CSI phase difference data to remotely detect breathing and heart rates with commodity WiFi devices. It can achieve a higher estimation accuracy of vital signs, with easy, low-cost deployment. This work also provides a rigorous analysis of the CSI phase data, and proves that the phase difference data is periodic and has the same frequency as the breathing signal.

VI. Conclusions

In this paper, we presented PhaseBeat to exploit CSI phase difference data to monitor breathing and heartbeats with commodity WiFi device. We first provided a rigorous analysis of CSI phase difference data, with respect to its stability and periodicity. We then described the PhaseBeat design in detail, including environment detection, data calibration, subcarrier selection, and discrete wavelet transform. We implemented PhaseBeat with off-the-shelf WiFi devices, and conducted an extensive experimental study with three setups. The experimental results showed that PhaseBeat can achieve superior performance on breathing and heart rate detection over existing methods.

ACKNOWLEDGMENT

This work is supported in part by the US NSF under Grant CNS-1702957, and through the Wireless Engineering Research and Education Center at Auburn University.

REFERENCES

[1] O. Boric-Lubeke and V. Lubecke, "Wireless house calls: using communications technology for health care and monitoring," *IEEE Microwave Mag.*, vol. 3, no. 3, pp. 43–48, 2002.

[2] C. Hunt and F. Hauck, "Sudden infant death syndrome," *Can. Med. Assoc. J*, vol. 174, no. 13, pp. 1309–1310, 2006.

[3] M. L. R. Mogue and B. Rantala, "Capnometers," *Journal of Clinical Monitoring*, 1988.

[4] N. H. Shariati and E. Zahedi, "Comparison of selected parametric models for analysis of the photoplethysmographic signal," in *Proc. 1st IEEE Conf. Comput., Commun. Signal Process.*, Kuala Lumpur, Malaysia, Nov. 2005, pp. 169–172.

[5] F. Adib, H. Mao, Z. Kabelac, D. Katabi, and R. Miller, "Smart homes that monitor breathing and heart rate," in *Proc. ACM CHI'15*, Seoul, Korea, Apr. 2015, pp. 837–846.

[6] A. Droitcour, O. Boric-Lubecke, and G. Kovacs, "Signal-to-noise ratio in doppler radar system for heart and respiratory rate measurements," *IEEE Trans. Microw. Theory Technol.*, vol. 57, no. 10, pp. 2498–2507, Oct. 2009.

[7] P. Nguyen, X. Zhang, A. Halbower, and T. Vu, "Continuous and fine-grained breathing volume monitoring from afar using wireless signals," in *Proc. IEEE INFOCOM'16*, San Francisco, CA, Apr. 2016.

[8] J. Salmi and A. F. Molisch, "Propagation parameter estimation, modeling and measurements for ultrawideband mimo radar," *IEEE Trans. Microw. Theory Technol.*, vol. 59, no. 11, pp. 4257–4267, Nov. 2011.

[9] Z. Yang, P. Pathak, Y. Zeng, X. Liran, and P. Mohapatra, "Monitoring vital signs using millimeter wave," in *Proc. IEEE MobiHoc'16*, Paderborn, Germany, July 2016.

[10] H. Abdelnasser, K. A. Harras, and M. Youssef, "Ubibreathe: A ubiquitous non-invasive wifi-based breathing estimator," in *Proc. IEEE MobiHoc'15*, Hangzhou, China, June 2015, pp. 277–286.

[11] D. Halperin., W. J. Hu., A. Sheth., and D. Wetherall., "Predictable 802.11 packet delivery from wireless channel measurements," in *Proc. ACM SIGCOMM'10*, New Delhi, India, Sept. 2010, pp. 159–170.

[12] Y. Xie, Z. Li, and M. Li, "Precise power delay profiling with commodity wifi," in *Proc. ACM MobiCom'15*, Paris, France, Sept. 2015, pp. 53–64.

[13] J. Liu, Y. Wang, Y. Chen, J. Yang, X. Chen, and J. Cheng, "Tracking vital signs during sleep leveraging off-the-shelf wifi," in *Proc. ACM MobiHoc'15*, Hangzhou, China, June 2015, p. 267276.

[14] Z. Yang, Z. Zhou, and Y. Liu, "From RSSI to CSI: Indoor localization via channel response," *ACM Comput. Surv.*, vol. 46, no. 2, Nov. 2013.

[15] J. Xiong and K. Jamieson, "Arraytrack: A fine-grained indoor location system," in *Proc. ACM NSDI'13*, Lombard. IL, Apr. 2013, pp. 71–84.

[16] M. Speth, S. Fechtel, G. Fock, and H. Meyr, "Optimum receiver design for wireless broad-band systems using OFDM–Part I," *IEEE Trans. Commun.*, vol. 47, no. 11, pp. 1668–1677, Nov. 1999.

[17] J. Gjengset, J. Xiong, G. McPhillips, and K. Jamieson, "Phaser: Enabling phased array signal processing on commodity WiFi access points," in *Proc. ACM MobiCom'14*, Maui, HI, Sept. 2014, pp. 153–164.

[18] S. Sardy, P. Tseng, and A. Brace, "Robust wavelet denoising," *IEEE Trans. Signal Process.*, vol. 49, no. 6, pp. 1146–1152, Jun. 2001.

[19] B. D. Rao and K. V. S. Hari, "Performance analysis of root-music," *IEEE Trans. Acoust., Speech, Signal Process.*, vol. 37, no. 12, pp. 1939–1949, Dec. 1989.

[20] C. G. Scully, J. Lee, J. Meyer, A. M. Gorbach, D. Granquist-Fraser, Y. Mendelson, and K. H. Chon, "Physiological parameter monitoring from optical recordings with a mobile phone," *IEEE Trans. Biomed. Eng.*, vol. 59, no. 2, pp. 303–306, Feb. 2010.

[21] H. Aly and M. Youssef, "Zephyr: Ubiquitous accurate multi-sensor fusion-based respiratory rate estimation using smartphones," in *Proc. IEEE INFOCOM'16*, San Francisco, CA, Apr. 2016, pp. 1–9.

[22] Y. Ren, C. Wang, J. Yang, and Y. Chen, "Fine-grained sleep monitoring: Hearing your breathing with smartphones," in *Proc. IEEE INFOCOM'15*, Hong Kong, China, Apr. 2015, pp. 1194–1202.

[23] X. Wang, C. Yang, and S. Mao, "TensorBeat: Tensor decomposition for monitoring multi-person breathing beats with commodity WiFi," in *ACM Trans. on Intelligent Systems and Technology*.

[24] X. Wang, L. Gao, and S. Mao, "BiLoc: Bi-modality deep learning for indoor localization with 5GHz commodity Wi-Fi," in *IEEE Access J.*, to appear. DOI: 10.1109/ACCESS.2017.2688362.

[25] X. Wang, X. Wang, and S. Mao, "CiFi: Deep convolutional neural networks for indoor localization with 5GHz Wi-Fi," in *Proc. IEEE ICC 2017*, Paris, France, May. 2017.

[26] X. Wang, L. Gao, S. Mao, and S. Pandey, "CSI-based Fingerprinting for Indoor Localization: A Deep Learning Approach," *IEEE Trans. Veh. Technol.*, vol.66, no.1, pp.763–776, Jan. 2017.

[27] X. Wang, L. Gao, and S. Mao, "CSI phase fingerprinting for indoor localization with a deep learning approach," *IEEE Internet of Things J.*, vol.3, no.6, pp.1113–1123, Dec. 2016.